A procedure for 3-D sight distance evaluation using thin plate splines

Dae Gun Kim
Department of Civil and Environmental Engineering
University of Maryland
1173 Martin Hall
College Park, MD 20742
E-mail: peeres@umd.edu

David J. Lovell
Department of Civil and Environmental Engineering
University of Maryland
1173 Martin Hall
College Park, MD 20742
Phone: 301-405-7995
E-mail: lovell@umd.edu

Submission date: October 16, 2009

Word count:	5226
Figures: 9 x 250	2250
Tables: 0 x 250	0
Total:	7476

ABSTRACT

This paper demonstrates an algorithm for measuring sight distance along a 3-D description of a roadway environment. The roadway is defined as a mesh of coordinates considering horizontal and vertical design elements, as well as cross-sectional elements including any crown slopes, superelevation, shoulders, clear zone, and lateral sight obstacles such as foliage or buildings.

Methods of computational geometry and an analogy to the structural mechanics of thin plates are used to determine the maximum available sight distance from any point on the alignment. The sight distance can be measured with the same resolution as that with which the geometric data were specified. The algorithm could easily be incorporated into software designed to do geometric consistency audits, road safety audits, or automated highway design.

The algorithm is tested against some sample alignment data, and the results are compared against traditional 2-dimensional procedures.

1. Introduction

This paper addresses the issue of measuring, for an arbitrary alignment defined in three dimensions of space, the available sight distance from any point on the alignment in either direction. This information can then be used to help determine appropriate design and posted speeds, locations of no-passing zones, and zones where further design revisions may be necessary in order to bring the alignment up to the desired standard.

Sight distance is normally considered in two-dimensional planes. The standard views of a highway alignment include the plan view, which is a two-dimensional projection of the 3-D alignment onto the *x-y* plane, and the profile view, which is a projection of the elevation and arclength along the road onto a vertical plane. Both views can be exploited to give an estimate of sight distance, and standard practice is to construct these estimates, and then use the minimum of the two at each point as a conservative estimate. The problem with this approach is that, since both projections are missing information from the overall 3-D alignment, there are geometric configurations in which this procedure yields incorrect results. The goal of this paper is to construct a new three-dimensional sight distance model that considers both horizontal and vertical alignment factors simultaneously and that deals with other necessary factors (e.g. shoulder, clear zone, vertical factors of continuous lateral obstructions) for highway alignments. The remainder of Section 1 of this paper describes previous sight distance studies and the specific objectives of this paper.

The review of the literature is divided into four sections according to types of sight distance. In the first section, horizontal sight distance models are described. The research related to vertical sight distance follows in the second section. In the third section, three-dimensional algorithms are reviewed. Finally, the reviews of the literature are summarized in the fourth section, focusing on the problems and limitations of the previous work.

1.1 Two - Dimensional Horizontal Sight Distance

On horizontal curves, a driver's sight distance is presumed to be blocked by an obstruction which is located outside of the traveled way. The AASHTO Green Book (2) provides a 2-dimensional sight distance model. This model assumes that both ends of the sight line are on the same horizontal curve. Numerous improvements have been suggested in the literature. The Green Book itself suggests that graphical methods be used for more complicated situations, which is unfortunate, since more robust analytical methods exist.

Hassan et al. (3) studied the relationships between various combinations of horizontal geometric elements and single or multiple obstacles. He developed exact formulae for sight distance in these situations with arbitrary locations of the observer (driver) and obstacle. Similar efforts (4, 5) include compound curves and reverse curves. Up to that point, spiral curves and continuous obstacles were not considered. Hassan et al. (1) developed general analytical methods to calculate available sight distance for continuous obstacles and for horizontal alignments including spiral design elements.

Lovell (6) and Lovell et al. (7) developed a set of algorithms to determine sight distance for an arbitrary sequence of all of the commonly used horizontal design elements, with a continuous obstruction line at variable distances from the centerline. These papers include two primary contributions – a set of expressions for determining the vector-valued functions of centerline position (and any parallel curves), and an algorithm for determining 2-D sight distance in this geometric plane. The 2-D expressions from that work will be used as the basis for the 2-D portion of the roadway geometry in this effort, and it will be extended with similar formulae for the vertical component of each of the vectors.

1.2 Two - Dimensional Vertical Sight Distance

Sight distance is the major control over the design of vertical components of roadway design (2). Again, the recipes provided in the design manual are appropriate only to the most basic alignment configurations, and only when both the driver and the obstacle are on the same curve, which is only a small fraction of the cases one would want to investigate to construct a complete sight distance profile.

Easa (8, 9) suggested vertical sight distance models for a broader class of vertical curves, including unsymmetrical sag curves and unsymmetrical crest curves. These new methods also consider driver and obstacle positions that are beyond the range of the vertical curve itself.

1.3 Three - Dimensional Sight Distance

It is widely recognized that coincidental combinations of horizontal and vertical curvature can render each of the projection-based sight distance methods inaccurate. The notion of applying both methods and then adopting the worst measurement of the two, while certainly an improvement, is also inaccurate. The best approach would be to consider both forms of curvature simultaneously, using a 3-dimensional representation of the roadway alignment and the accompanying mathematical devices. This is what is meant by publications (including the Green Book) that advocate a “graphical method”; however, this suggestion implies that these problems are not tractable analytically, which is not true.

Hassan (10) introduced an analytical three-dimensional model using the finite element method (FEM) whose elements are rectangular (4-node, 6-node, and 8-node) and triangular. His sight distance model is more advanced because it combines horizontal and vertical alignments. This method can also accommodate cross slopes and superelevation. Its primary contribution is in the mathematical expression of the roadway geometry; the sight distance computation is a cumbersome numerical search procedure.

Ismail (11) expanded the 2-D models in (6) and (7) to include a three-dimensional component. This was accomplished using piecewise linear approximations to all of the curvature elements. Nehate and Rys (12) used a different set of approximations, specifically cubic B-spline functions, to represent road and drivers’ positions into three-dimensional space. They also

dealt at some length with the constraint on sight distance imposed by the visibility cone of headlights at night.

1.4 Summary

An argument for considering horizontal and vertical sight distance computations separately is that these design elements rarely co-exist. It is not clear to what extent this presumption is true, although the authors are certainly aware of cases where it is not. The argument for a combined approach, then, is that it is mathematically tractable, it yields identical results to the planar methods when combined curvature does not exist, and it gives accurate results when it does exist. In short, such a method is universally applicable.

Graphical methods are useful for pedagogical purposes, but are not necessary as practical engineering tools, since mathematical and computational methods exist to do the job properly. This paper presents an analytical method for three-dimensional sight distance analysis that considers a very robust geometric description of the roadway, and an efficient computation scheme built on an analogy from structural mechanics.

2. Methodology

This section deals specifically with methods to compute available sight distance (ASD) in three dimensions. This is accomplished in three parts. The first part demonstrates exact functions for the horizontal and vertical alignment, in a 3D coordinate system. The horizontal alignment is based specifically on the methods in (6) and (7). The second part yield new three-dimensional functions for sight lines and other road elements (e.g., center line of a road, road surface, shoulder, clear-zone, and obstruction). Finally, focusing on the links between constraints and sight lines in the three dimensional plane, this paper suggests an efficient method to estimate ASD using an analogy to the structural mechanics of thin plates.

2.1 Alignment Geometry

The roadway alignment is specified as a set of sections, each of which has its own geometric parameters. Let L_i denote the length of section i. Distance is measured in arclength t along the centerline of the alignment, and section endpoints are given by the set t_k. The notation $l(k)$ denotes the distance from station t_{i-1} to an arbitrary station k, where $k \in [t_{i-1}, t_i]$.

This paper uses four geometric vector functions. First, $\mathbf{W}_z$ is a unit vector in the vertical direction used to express only elevation at a point.

$$\mathbf{W}_z = \begin{bmatrix} 0 \\ 0 \\ 1 \end{bmatrix} \tag{1}$$

Using 2D coordinates from references (6) and (7), $\mathbf{W}_w\ \alpha_i : \mathbb{R} \to \mathbb{R}^3$ is the vector-valued function whose image is the unit vector that makes an angle α_i with the x-axis in the x-y plane:

$$\mathbf{W}_w(\alpha_i) = \begin{bmatrix} \cos\alpha_i \\ \sin\alpha_i \\ 0 \end{bmatrix} \tag{2}$$

Similarly, $W_h\ \alpha_i\ : \mathbb{R}^3 \to \mathbb{R}^3$ is a rotation matrix that rotates any vector in $\mathbb{R}^3$ about the z-axis, through an angle of α_i:

$$W_h = \begin{bmatrix} \cos\alpha_i & -\sin\alpha_i & 0 \\ \sin\alpha_i & \cos\alpha_i & 0 \\ 0 & 0 & 1 \end{bmatrix} \tag{3}$$

Finally, horizontal alignments are allowed to include clothoid spirals for horizontal transition curves. Again from reference (6), with the use of Fresnel integrals, a direction vector $\mathbf{U}\ \delta_k$ of a clothoid curve can be expressed, as follows:

$$\mathbf{U}(\delta_k) = \begin{bmatrix} x_k \\ y_k \\ z_k \end{bmatrix} = \begin{bmatrix} S(\delta_k) \\ C(\delta_k) \\ 0 \end{bmatrix} = \begin{bmatrix} \int_0^{\delta_k} \sin(t^2)dt \\ \int_0^{\delta_k} \cos(t^2)dt \\ 0 \end{bmatrix} = \begin{bmatrix} \sum_{n=0}^{\infty} (-1)^n \frac{x^{4n+3}}{(4n+3)(2n+1)!} \\ \sum_{n=0}^{\infty} (-1)^n \frac{x^{4n+1}}{(4n+1)(2n)!} \\ 0 \end{bmatrix} \tag{4}$$

2.1.1 Vertical Alignment

This paper considers two vertical alignment elements – the tangent and the parabolic vertical curve. Other specialty elements could be admitted to the methodology with very little effort; if their geometry can be represented similar to what is done in this section, then the remaining sight distance estimation procedure can be applied as-is.

Tangent Section

The angle between the x-y plane and the 3-D tangent vector at the start of section *i* is denoted by β_i. The same angle is in effect at the end of the tangent section; thus is section *i* is a vertical tangent, then $\beta_{i+1} = \beta_i$. The grade of the tangent section is $\tan\ \beta_i$. At a distance k into section I, the vertical component of the roadway can be given as:

$$z_k = z_{i-1} + \ t_k - t_{i-1}\ \tan\ \beta_i \tag{5}$$

Parabolic Section

Following standard convention, distance along the length of a vertical parabolic curve is measured along its projection onto the horizontal plane, since grades are almost always quite small. The parabola is parameterized by its initial grade (β_i), its length L_i, and its change in grade $A_i = \beta_{i+1} - \beta_i$. The expression for the vertical component along the parabola is:

$$z_k = z_{i-1} + \ t_k - t_{i-1} \left(\tan\beta_i + \frac{A_i}{2L_i}\ t_k - t_{i-1} \right) \tag{6}$$

2.1.2 Horizontal Alignment

There are three basic types of horizontal section considered in this paper; tangent, circular curve, and clothoid spiral curve. Although there are other types of horizontal curve (e.g., compound

curves), they are composed from the three basic types. The geometry of the horizontal elements is taken directly from references (6) and (7).

Tangent section

At the beginning of section *i*, the horizontal alignment makes an angle α_i with the *x*-axis in the *x-y* plane. Since a tangent section does not effect a change in this angle, $\alpha_{i+1} = \alpha_i$. At an arbitrary point t_k within the section, the vector $\mathbf{S}_k$ points to that location in the *x-y* plane, where $\mathbf{S}_i$ was a similar vector pointing to the beginning of the section:

$$\mathbf{S}_k = \mathbf{S}_i + \ t_k - t_i \ \ \mathbf{W}_W \ \ \alpha_i \tag{7}$$

A proper 3-D vector for that, or any other point in this paper, is then given by:

$$\mathbf{X}_k = \mathbf{S}_k + z_k \mathbf{W}_z \tag{8}$$

Circular Section

If section *i* is a circular curve, then it has radius r_i. An *x-y* vector that points from the center of the circle to the start point of the section is given by:

$$\mathbf{V}_i = r_i \mathbf{W}_w \left(\alpha_i - \frac{\pi}{2} dir_i \right) \tag{9}$$

where dir_i denotes the direction in which the curve is turning, 1 if the curve rotates counter-clockwise along its length, and -1 if clockwise. The center of the circle is then given by:

$$\mathbf{C}_i = \mathbf{S}_i - \mathbf{V}_i \tag{10}$$

Any point t_k along the circle can be identified by:

$$\mathbf{S}_k = \mathbf{C}_i + W_h \left(dir_i \frac{t_k - t_i}{r_i} \right) \mathbf{V}_i \tag{11}$$

A circular curve changes the tangent angle according to:

$$\alpha_{i+1} = \alpha_i + dir_i \frac{L_i}{r_i} \tag{12}$$

Spiral Curve Section

Clothoid spiral curves are used most often to transition between horizontal tangents and circular curves, in which cases one end of the spiral has zero curvature. In some cases, they can also be used to transition between two consecutive circular curves having different ending curvature. The former cases can be called "complete" spirals, and the latter "partial" spirals, and their geometry is derived in detail in (6) and (7), respectively.

The beginning curvature κ_i of an increasing complete spiral is equal to zero because its previous section is tangent. Denote by δ_i the spiral angle, which is the difference in tangent angle between the beginning and end of the spiral curve. Then the ending curvature is given by:

$$\kappa_{i+1} = 2 \frac{\delta_i}{L_i} \tag{13}$$

At a point at location t_k the angular change is given by:

$$\delta_k = dir_i \frac{t_k - t_i^{\ 2} \kappa_{i+1}}{2L_i} \tag{14}$$

and the vector to the point itself can be located as follows:

$$\mathbf{S}_k = \mathbf{S}_i + \ t_k - t_i \ W_h(\alpha_i)\mathbf{U}(\delta_k) \tag{15}$$

The geometry of the decreasing complete spiral is similar, but the perspective is that of an increasing spiral looking backwards. In this case, the ending curvature κ_{i+1} is zero. The beginning curvature was κ_i, equal to whatever curvature prevailed at the end of the previous section. The angular change at location t_k is given by:

$$\delta_k = dir_i \frac{(L_i - t_k)^2 \kappa_i}{2L_i} \tag{16}$$

The location vector at this point is given by:

$$\mathbf{S}_k = \mathbf{S}_i + L_i W_h(\alpha_i)\mathbf{U} \ -dir_i\delta_k \ -(L_i - t_k)W_h(\alpha_i)\mathbf{U}(-\delta_k) \tag{17}$$

Lovell et al. (7) derived the geometry for partial spirals by first determining the geometry of the hypothetical complete spiral that the given curve would have been a part of, and deducing from that the geometry of the "missing spiral," being the difference between the two, which is itself a complete spiral of shorter arclength. Then, the results from equations (13)-(17) are combined to produce the proper results.

If the radii of curvature at both ends of the partial spiral are r_{i_1} and r_{i_2}, then the length of the hypothetical complete spiral is:

$$L_S = \frac{L_i \max \ r_{i_1}, r_{i_2}}{\left| r_{i_1} - r_{i_2} \right|} \tag{18}$$

and the length of the missing spiral is $L_m = L_S - L_i$. The spiral angle of the complete spiral is:

$$\delta_S = \frac{dir_i L_S}{2 \min \ r_{i_1}, r_{i_2}} \tag{19}$$

And the spiral angle of the missing spiral is $\delta_m = \delta_S - \delta_i$. For an increasing partial spiral, an arbitrary point at distance t_k is given as:

$$\mathbf{S}_k = \mathbf{S}_i - L_m W_h \ \alpha_i - \delta_m \ \mathbf{U} \ \delta_m \ + \ L_m + t_k - t_i \ W_h \ \alpha_i - \delta_m \ \mathbf{U}\left(\frac{dir_i \ L_m + t_k - t_i^{\ 2}}{2 r_{i_2} L_S} \right) \tag{20}$$

Similarly, for a decreasing partial spiral, the location vector is given as:

$$\mathbf{S}_k = \mathbf{S}_i - L_S W_h \ \alpha_i + \delta_S - \pi \ \mathbf{U} \ -\delta_S \ + \ L_S - t_k + t_i \ W_h \ \alpha_i + \delta_S - \pi \ \mathbf{U}\left(\frac{-dir_i \ L_S - t_k + t_i^{\ 2}}{2 r_{i_1} L_S} \right) \tag{21}$$

2.2 Roadway Elements

The methods of the previous section can be used to fix the location of the roadway centerline at any given point along the alignment. At any such point, a plane can be defined that is normal to the tangent vector at that point. All other roadway elements, referenced to this point on the centerline, can be located in this plane, including the edge of the road surface, the shoulders, clear zones, and obstructions. The position vector at any point t_k is denoted $\mathbf{X}_k$, the tangent vector $\mathbf{T}_k$, and the normal vector $\mathbf{N}_k$.

Considering only points of interest on the right hand side, the position of the edge of the driveable pavement surface is $\mathbf{A}_k$, and the outer edge of the shoulder is $\mathbf{B}_k$, which is also the start point of the clear zone. The nearest point of an obstacle is $\mathbf{C1}_k$ and the far edge is $\mathbf{C0}_k$. Figure 1 shows visually the configuration and notation of all of these elements.

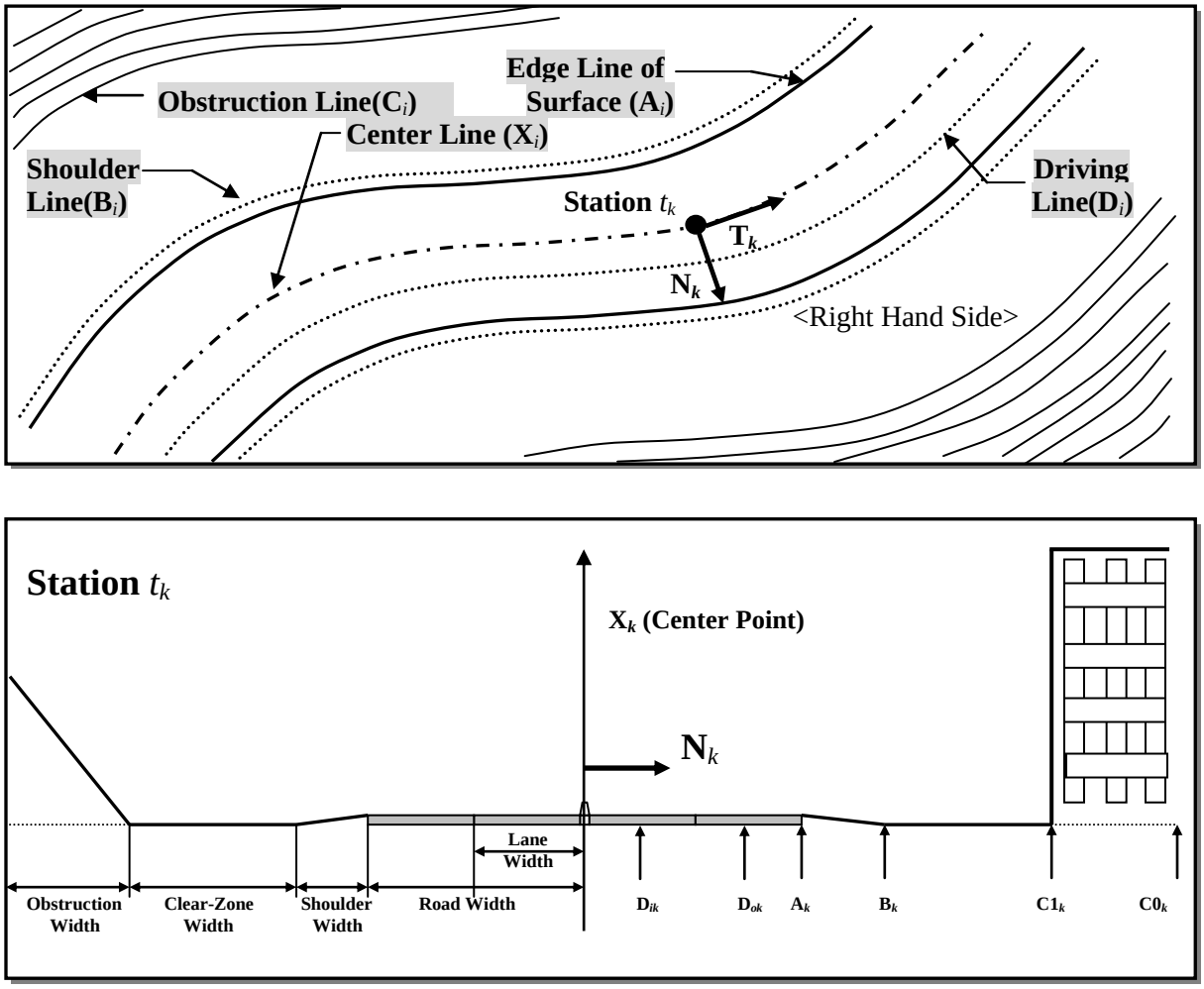

Figure 1. Highway Dimensions

This methodology includes consideration of superelevation and superelevation transitions in the set of lateral design elements that can be applied at each point on the centerline. The point $\mathbf{A}_k$ is given geometrically as:

$$\mathbf{A}_k = \mathbf{X}_k + n_k w_k W_h \left(\frac{(-1)^m \pi}{2} \right) \mathbf{T}_k + n_k w_k \left(e_i + \ t_k - t_i \ \left(\frac{e_{i+1} - e_i}{L_i} \right) \right) \mathbf{W}_z \tag{22}$$

where n_k is the number of lanes on one side of the centerline, w_k is the width of each lane, and e_i and e_{i+1} are the superelevation rates at the beginning and end of the section, respectively. When the right edge is being considered, *m* should be set to zero; for the left edge, $m = 1$.

Shoulder

The position of the edge of the shoulder at station *k*, $\mathbf{B}_k$, can be derived from $\mathbf{A}_k$. If s_k is the shoulder width, and sg_i and sg_{i+1} are the shoulder grades at the beginning and end of the section, respectively, then the point $\mathbf{B}_k$ is given as:

$$\mathbf{B}_k = \mathbf{A}_k + s_k W_h \left(\frac{(-1)^m \pi}{2} \right) \mathbf{T}_k + s_k \left(sg_i + \ t_k - t_i \ \left(\frac{sg_{i+1} - sg_i}{L_i} \right) \right) \mathbf{W}_z \tag{23}$$

Clear-Zone

The clear zone is a flat area outside of the shoulder that should be clear of all driving and visibility obstacles to provide an escape area for vehicles leaving the roadway, as well as clearance for sight lines around horizontal curves. If the width of the clear zone is c_k, then the location of the end of the clear zone can be written as:

$$\mathbf{C1}_k = \mathbf{B}_k + c_k W_h \left(\frac{(-1)^m \pi}{2} \right) \mathbf{T}_k \tag{24}$$

Obstructions

The end of the clear zone is the first point where it is reasonable to include an obstacle. In preliminary design, very little is known about what type of obstacle might be present here, so for sight distance purposes, it is common to assume the worst-case scenario, which is a tall vertical obstacle. When more specific information is available, however, this can be included in the analysis. In this paper, we consider a variety of facing angles for the obstacle. Whenever it is not vertical, this allows for some opportunity for increased sight distance, depending on the surrounding geometry. The vertical angle of the obstacle is denoted γ. When considering earthwork cross-sections, it can be imagined that sections with $\gamma < 0$ are fill sections, and when $\gamma > 0$ they are cut sections, with $\gamma = 90^\circ$ reserved for buildings, signs, foliage, etc.

If o_k is the obstacle width, then the outer edge of the obstacle is given as:

$$\mathbf{C0}_k = \mathbf{C1}_k + o_k W_h \left(\frac{(-1)^m \pi}{2} \right) \mathbf{T}_k + o_k \tan \ \gamma_k \ \ \mathbf{W}_z \tag{25}$$

2.3 Thin Plate Spline

Given a set of station numbers at which all of the geometric points are identified, the result of the above methods is a mesh of points that define the envelope of the roadway and obstacle surface.

To measure sight distance in this environment, it is necessary to have an interpolating function that conforms (as well as possible) to these points, but is also defined at any intermediate point, essentially to turn the roadway surface into a continuum. A number of methods are possible for this, including polygonal finite elements (10), cubic B-splines (12), and perhaps others. In this paper, we adopt the method of thin plate splines (TPS) (13,14), which has the advantage over finite elements of producing a smooth interpolating function. The advantage over cubic B-splines is that a wider range of contiguous sections governs the local behavior of the function, and that reliable (i.e., bounded) behavior of the function can be expected outside of the range of the data for which it was estimated.

The physical analogy being modeled with TPS is that of fitting a thin flexible plate to the finite mesh of points described above, while minimizing the bending energy stored in the plate in that configuration. This method will produce a smooth function that matches, to the extent possible, every point in the mesh, and interpolates points between and beyond these points. The errors are bounded, both within and outside of the mesh.

The bending energy can be written as:

$$I_f = \iint_{R^2} \left\{ \left(\frac{d^2 z}{dx^2} \right)^2 + 2 \left(\frac{d^2 z}{dxdy} \right)^2 + \left(\frac{d^2 z}{dy^2} \right)^2 \right\} dxdy \tag{26}$$

This function is also called the "integral quadratic variation" or the "integral bending norm." To minimize the bending energy, the fundamental solution of the bi-harmonic equation should be equal to zero.

$$\Delta^2 z(x, y) = \left(\frac{d}{dx^2} + \frac{d}{dy^2} \right)^2 z(x, y) = 0 \tag{27}$$

The thin plate spline basis function is given as

$$U(r) = -r^2 \log(r) \tag{28}$$

With these facts, Bookstein (14) explained the way to formulate the TPS for an arbitrary set of landmarks. Suppose there are *n* geometric control points derived in Section 2.2 and write their *x*-*y* projections in some order $\mathbf{P}_i = x_i, y_i$. The distance between points *i* and *j* can then be written $r_{ij} = \left| \mathbf{P}_i - \mathbf{P}_j \right|$. We now construct the $n \times n$ matrix *K* containing the basis function information as:

$$K = \begin{bmatrix} 0 & U\ r_{12} & \cdots & U\ r_{1n} \\ U\ r_{21} & 0 & \cdots & U\ r_{2n} \\ \vdots & \vdots & \ddots & \vdots \\ U\ r_{n1} & U\ r_{n2} & \cdots & 0 \end{bmatrix} \tag{29}$$

and the $3 \times n$ matrix *P* containing the *x*-*y* planar geometry as:

$$P = \begin{bmatrix} 1 & x_1 & y_1 \\ 1 & x_2 & y_2 \\ \vdots & \vdots & \vdots \\ 1 & x_n & y_n \end{bmatrix} \tag{30}$$

Compose the block matrix

$$L = \left[\begin{array}{c|c} K & P \\ \hline P^T & 0 \end{array}\right] \tag{31}$$

where the lower right corner is a 3×3 matrix of zeros. Taking the original *z*-coordinates from the control points, form them into a column vector, augmented with three zeros, as:

$$\mathbf{Y} = \left[z_1, z_2, \ldots, z_n, 0, 0, 0 \right]^T \tag{32}$$

As shown in (14), the function $f(\cdot)$ that minimizes the bending energy can be written as:

$$f(x,y) = a_1 + a_x x + a_y y + \sum_{i=1}^{n} w_i U(|\mathbf{P}_i - (x,y)|) \tag{33}$$

where a_1, a_x, a_y, and the w_i are determined as the solution vector to the following linear system:

$$L^{-1}Y = \left[W \,\middle|\, a_1 \; a_x \; a_y \right]^T \tag{34}$$

2.4 Measuring Available Sight Distance

The previous sections formulate sight distance and surface constraints which include road surfaces and obstructions on the three-dimensional plane. This section describes how to calculate sight distance using these constraints.

For a driver at a given position along the alignment, a feasible sight line is a line that ends at some other position on the alignment (i.e., the "obstacle" position), and that remains above the 3-D profile of the alignment and its constraints throughout its length. One measures the available sight distance by finding the shortest sight line that violates this requirement, and then reducing the sight distance by one unit. Measurement of this sight distance is therefore an interated search. The following algorithm suffices to measure the sight distance at a point t_k along the alignment:

1. Set the driver's position as $\mathbf{X}_k$, and offset it if desired to the center of one of the travelled lanes using equation (22).
2. Set the end station number $\tau = k + \varepsilon$, where ε is the user-specified resolution with which to measure sight distance.
3. Construct the candidate sight line $\mathbf{L}_{k\tau}$ between $\mathbf{X}_k$ and $\mathbf{X}_\tau$, including vertical offsets for eye height and object height according to AASHTO (2).
4. If for every point ξ along $\mathbf{L}_{k\tau}$, $z\left(\mathbf{L}_{k\tau}(\xi)\right) > f\left(\mathbf{L}_{k\tau}(\xi)\right)$, where $f(\cdot)$ is determined by equation (33), then this is a feasible sight line, so set $\tau = \tau + \varepsilon$ and go back to Step 3 to continue the search.
5. Otherwise, this is the first *infeasible* sight line, so the previous one was the final feasible sight line. The endpoint of that sight line is $\mathbf{L}_{k,\tau-\varepsilon}$, and the sight distance at station t_k is $t_{\tau-\varepsilon} - t_k$, measured along the alignment arclength.

3. Case Study

This section describes a case study that illustrates the application of the new model, and compares it to what would have been obtained using common sight distance estimates available in the literature.

The alignment used for this case study is a real highway alignment slightly over a mile in length. The detailed alignment data are too voluminous to include here; they are available from the authors on request. The design speed of the road is 65 miles per hour, and it has two lanes in each direction. The coordinate geometry of the roadway is represented graphically in Figure 2. The scales differ to highlight the alignment features and Figure 2b is *not* the vertical profile, since the abscissa is measuring the actual *x*-coordinate rather than the arclength *t* along the alignment.

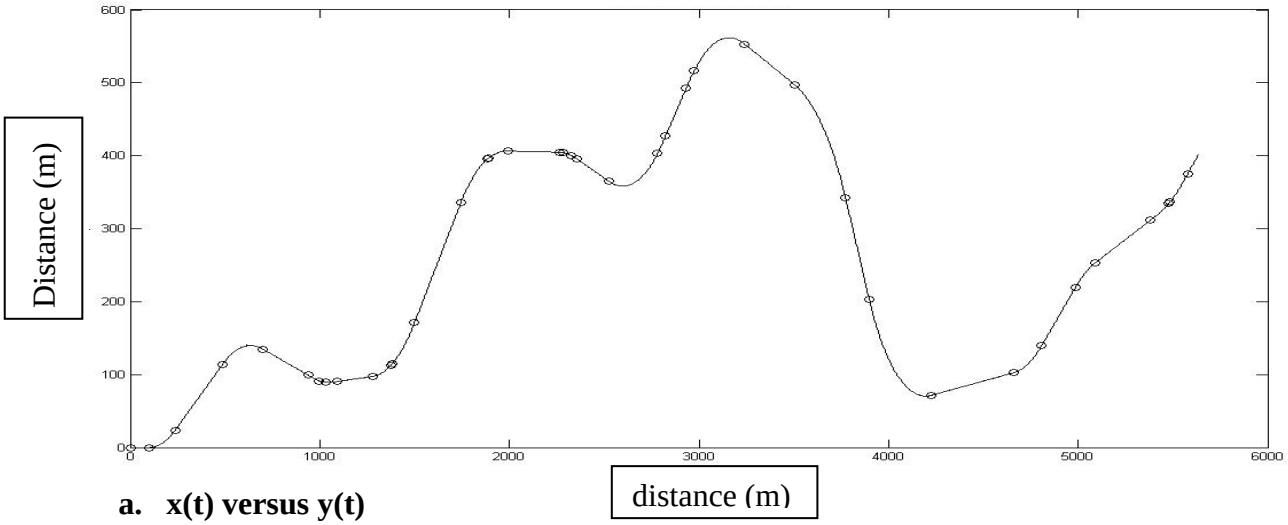

a. x(t) versus y(t)

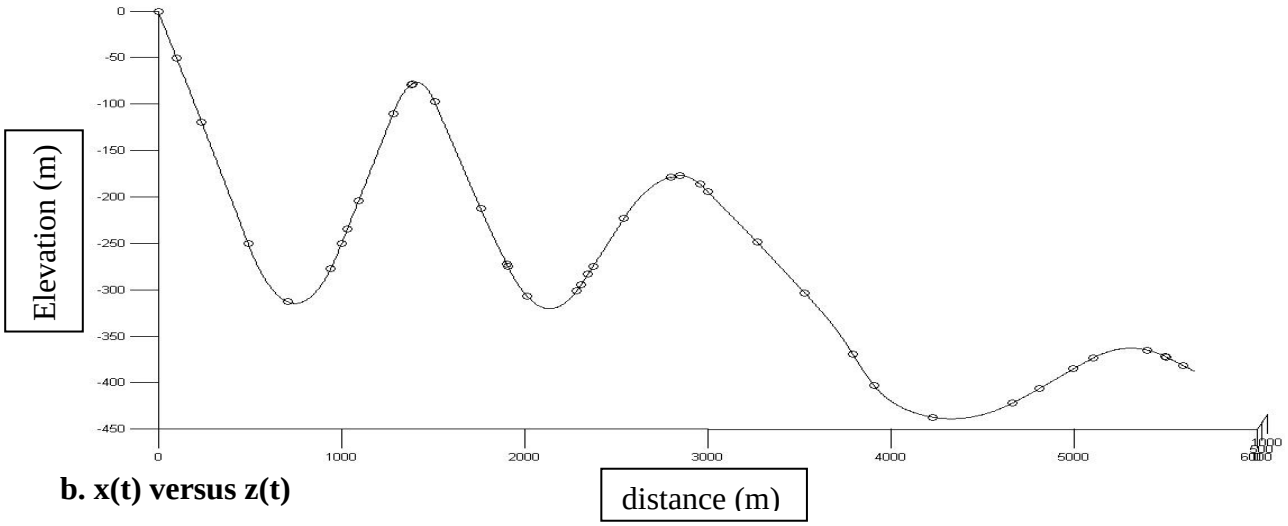

b. x(t) versus z(t)

Figure 2. Geometry of Example Alignment

Figure 3 shows the cross-slopes and shoulder slopes assumed throughout the alignment.

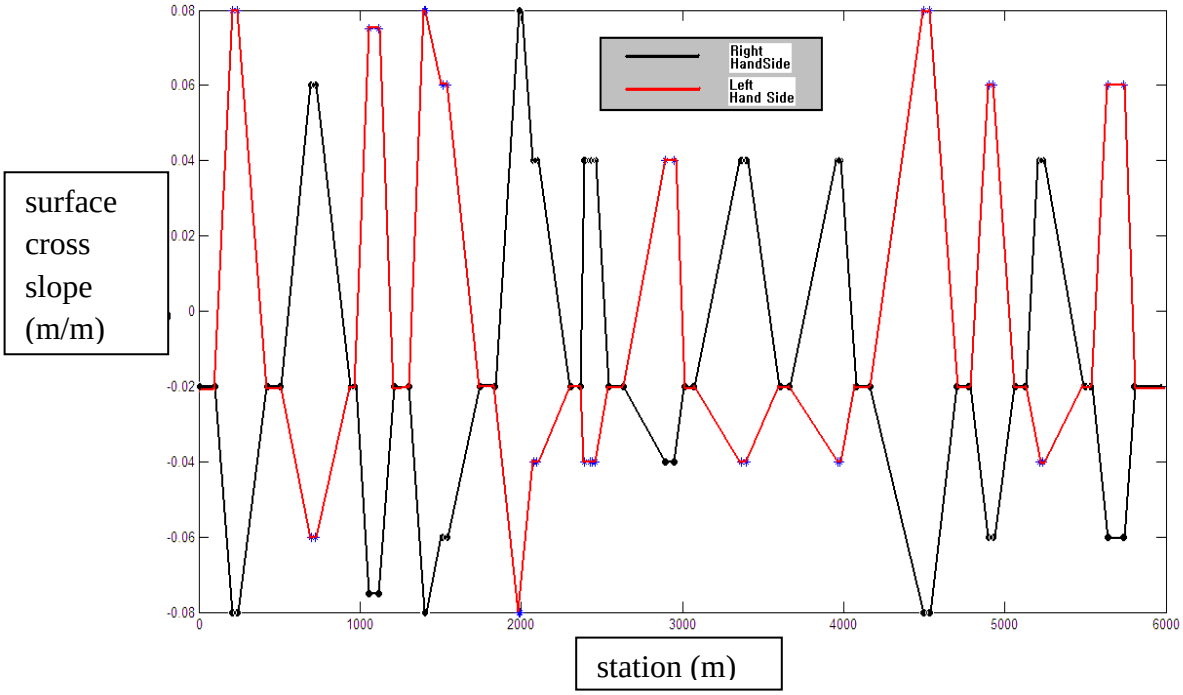

(a) Surface Cross Slopes on Example Alignment

station (m)

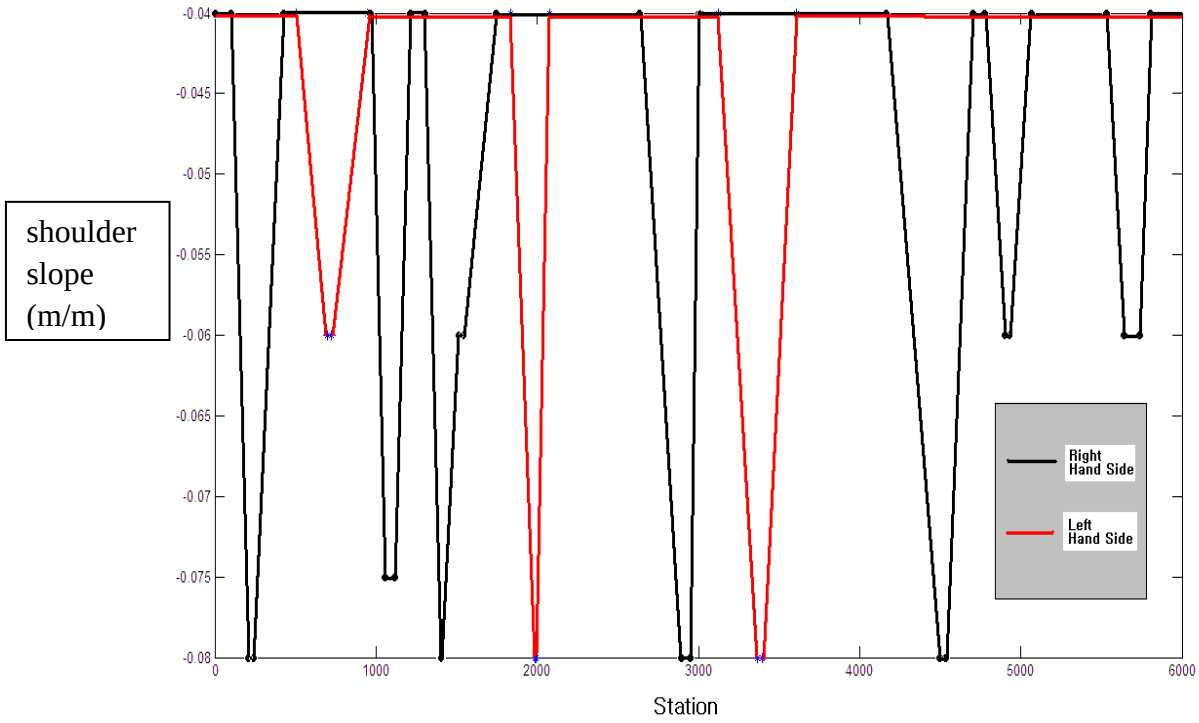

(b) Shoulder Slopes on Example Alignment

Figure 3. Surface and Shoulder Cross Slopes on Example Alignment

3.1 Thin Plate Spline

This alignment produces a huge number of geometric control points: 11,400 to be exact. This leads to several negative effects. First, the system is huge, so solving it takes time and introduces the chance for numerical solution errors due to ill conditioning of the matrices involved. Second, the magnitude of errors in the spline function can grow as the size of the problem grows. With a single spline function, the maximum vertical error was 35 cm. It makes sense, instead, to decompose the problem into smaller sub-problems. In this case, we used 39 sections, divided according to the type of horizontal alignment. Figure 4 shows the errors from a single thin plate spline.

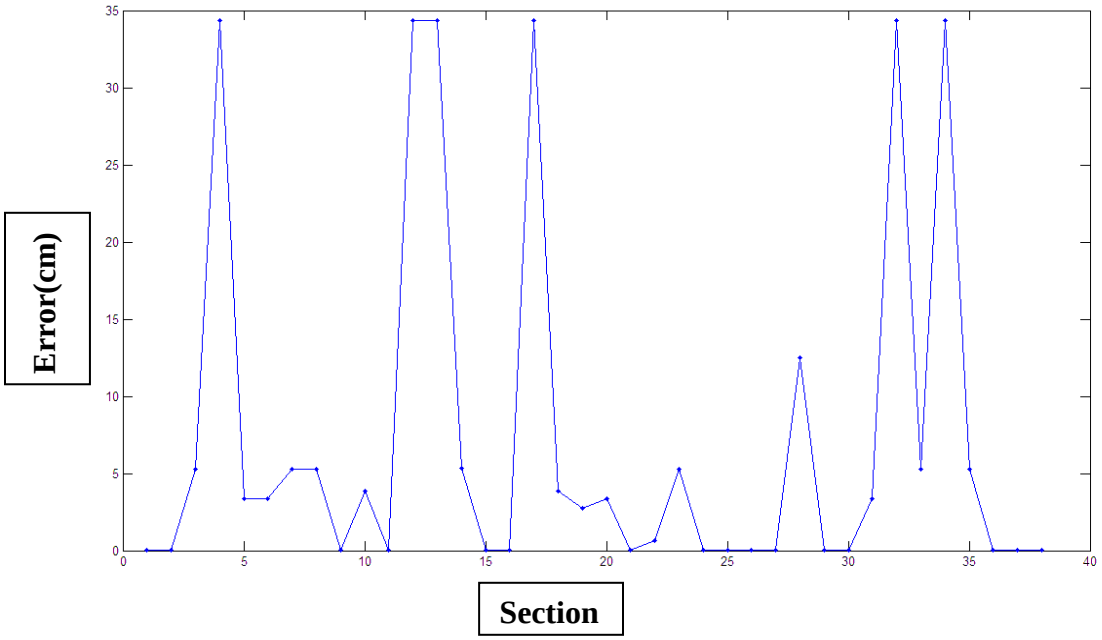

Figure 4. Vertical Errors with a Single TPS

It is best to break the alignment into sections that contain some overlap at each end, in order to constrain the independent thin plate splines in such a way that the results agree across subproblems. Upon investigation, all of the egregious errors in Figure 4 occurred where extreme values of the obstacles were defined. These values can be changed to more moderate values without fundamentally affecting the sight distance profile. After breaking the problem into subproblems, and correcting some of these extreme data, the error profile shown in Figure 5 was obtained.

3.2 Calculating Sight Distance

In this section, we show the results for the sight distance computations for a set of scenarios. In the first case, we consider only the horizontal geometry, in which case the sight distance results match exactly with what would have been predicted in the 2-D models of Lovell (6) and Lovell et al. (7). This is accomplished by setting all vertical grades to zero, allowing no vertical curves, superelevation, cross slopes, or shoulder slopes, and imposing extreme obstacle angles at the edge of the clear zone. Figure 6 shows a portion of the alignment constructed in this manner.

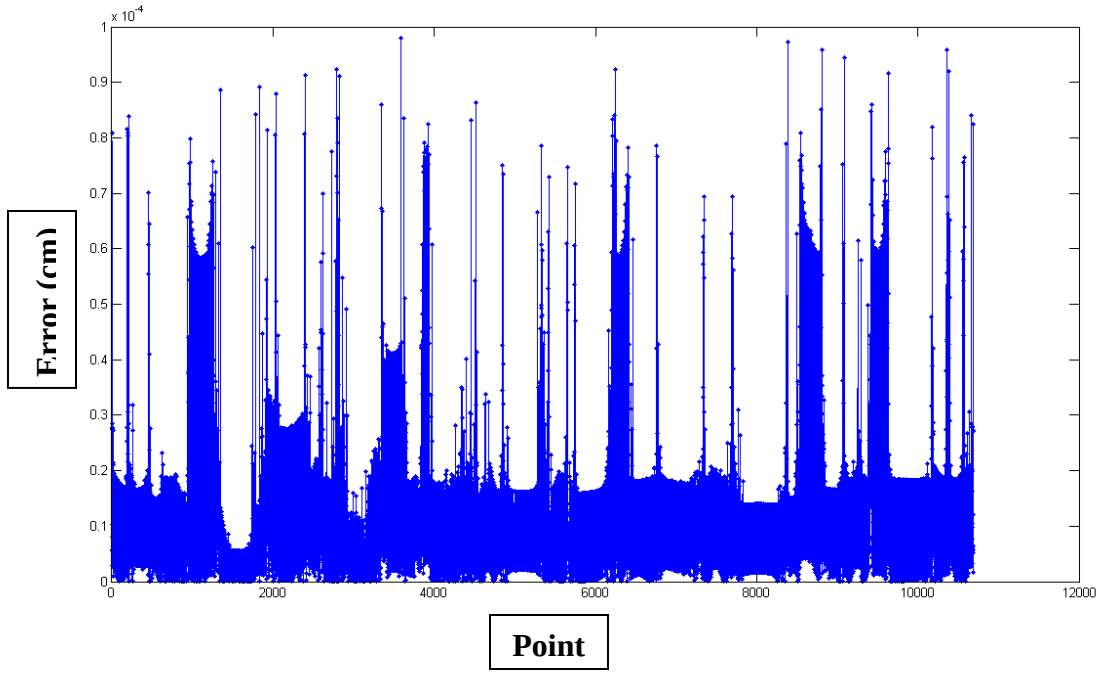

Figure 5. Vertical Errors with a Multiple Overlapping TPS

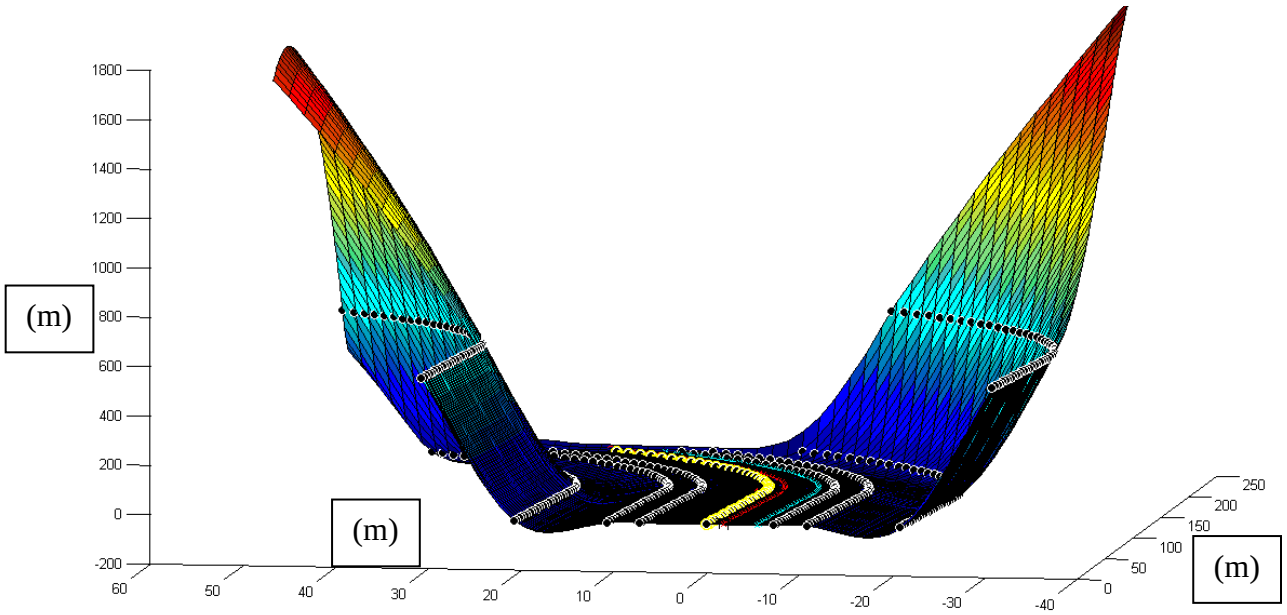

Figure 6. Road shape for Horizontal Sight Distance (Section 1 to 3)

A similar process can be followed to consider only vertical sight distance. In this case, what was required was the removal of all horizontal curvature elements, including circular curves and spirals. Figure 7 shows an example of what the "alignment" would look like with this simplification.

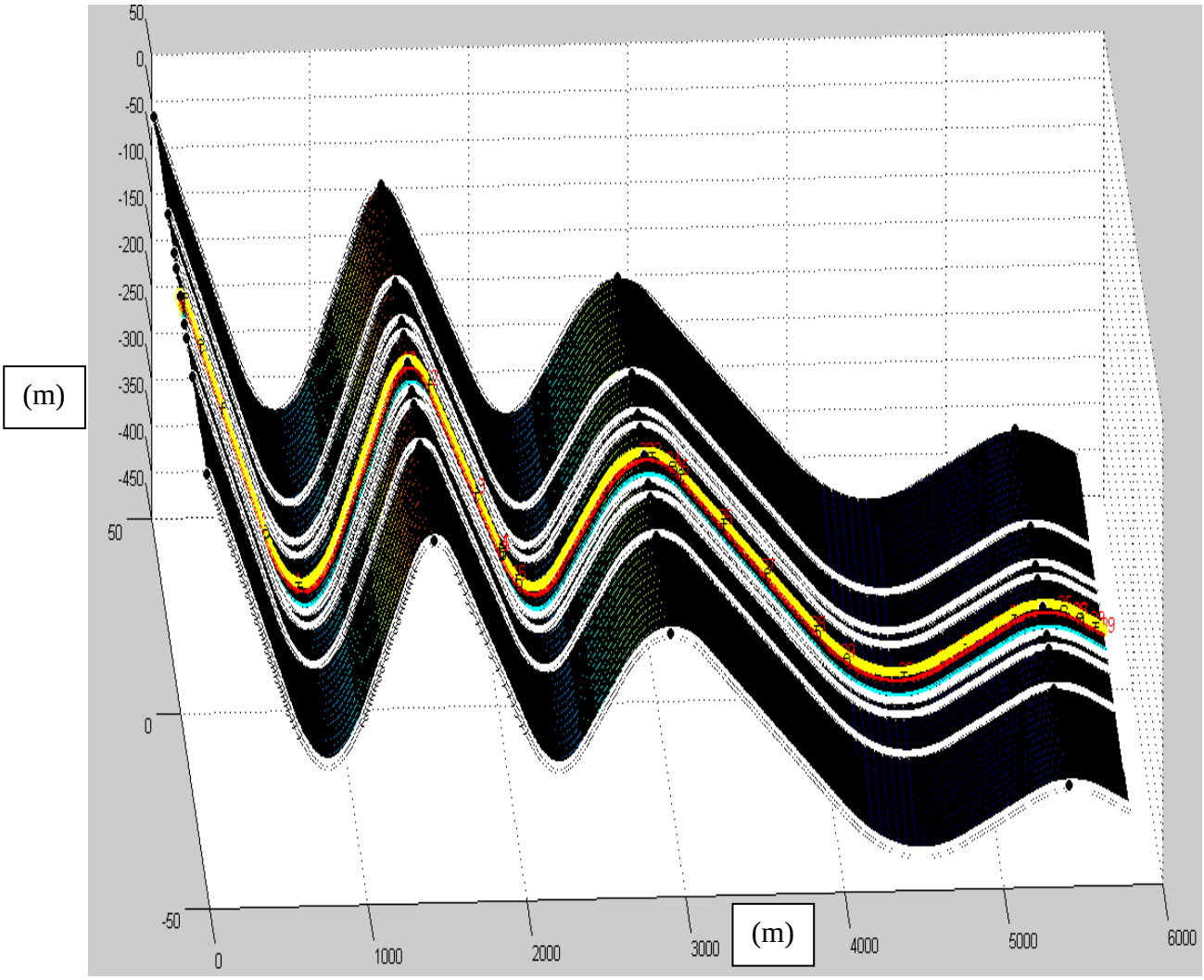

Figure 7. Road Shape for Vertical Sight Distance

Figure 8 shows the results for the sight distance computations involving only horizontal alignment and only vertical alignment. The figure also shows the minimum of the two curves, which represents the colloquial advice for producing 3-D sight distance estimates as given in references such as (2). The 2-D horizontal sight distance equation in reference (2), as mentioned previously, accounts only for circular curves, and assumes that both ends of the sight line are on the same curve, which does not actually happen that often. The equation for the sight distance in this situation is typically given as:

$$SD = 2r\cos^{-1}\left(1-\frac{m}{r}\right) \tag{35}$$

Where r is the curve radius, and m is the "middle ordinate," which for the present purposes can be thought of as the lateral distance between the start point of a lateral obstruction and the middle point of the outside lane.

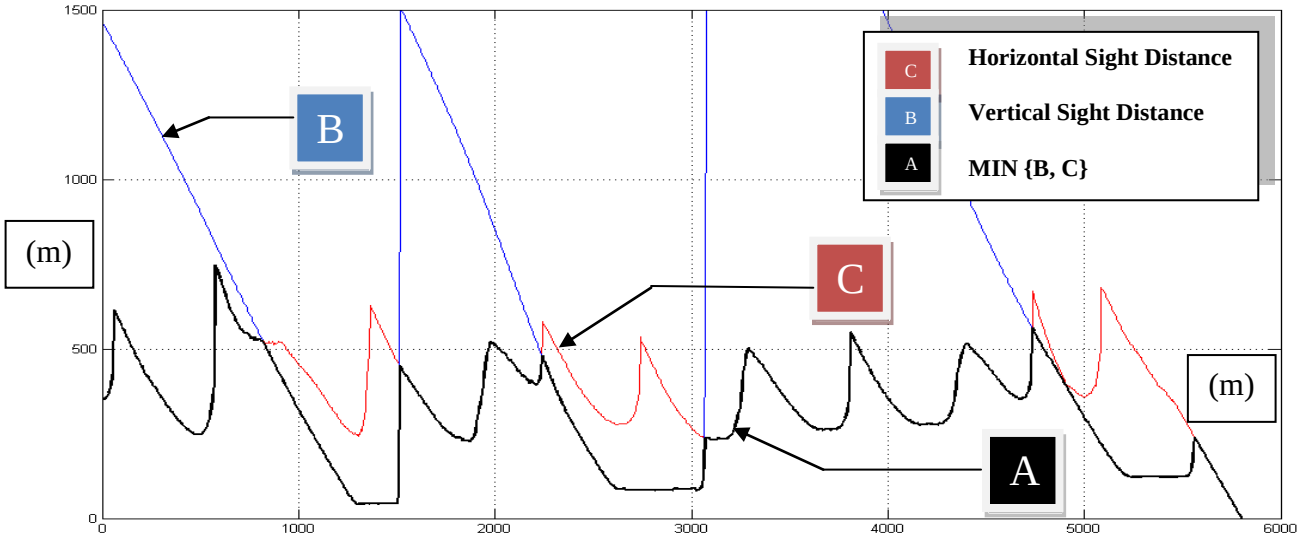

Figure 8. Horizontal and Vertical Sight Distance

Finally, Figure 9 shows the results comparing the new 3-D sight distance algorithm with the "old" 3-D sight distance algorithm representing the minimum of the horizontal and vertical results, as shown in Figure 8, along with the AASHTO sight distance results that would come from equation (35).

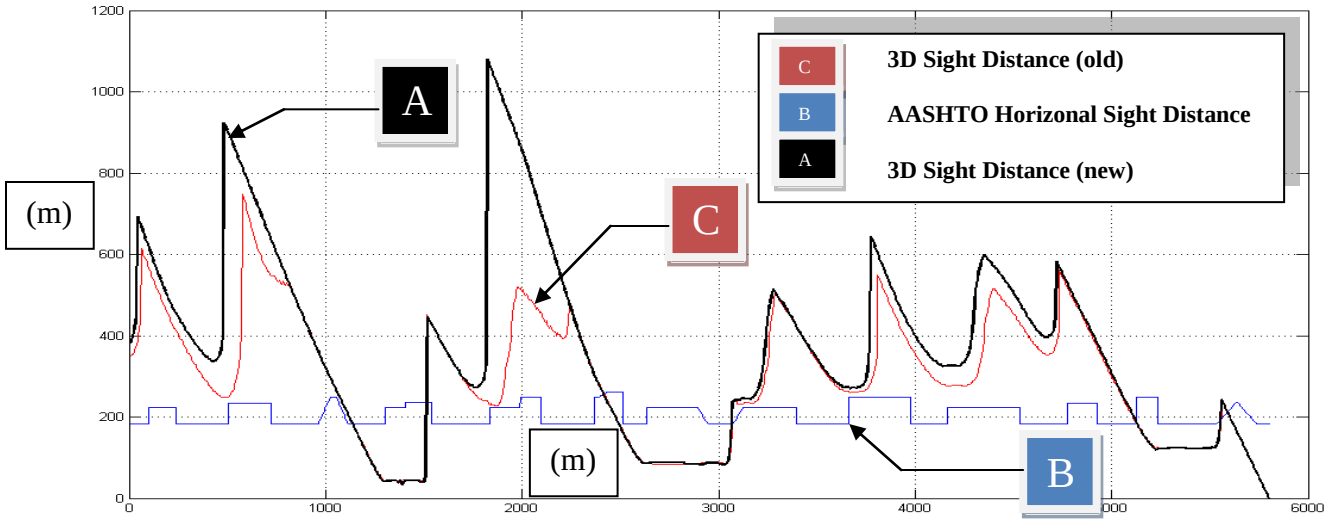

Figure 9. 3-D Sight Distance Comparisons

As this figure shows, the new sight distance algorithm agrees well in most places with the conventional recommendation, but allows for greater sight distance estimates in those places where the combination of horizontal and vertical alignment conspires to produce greater sight distance than would have been predicted otherwise. Both methods differ sharply from the AASHTO estimates, which is not surprising, given that the AASHTO estimates incorporate very little of the actual geometry of the roadway. Their only utility is the ease with which the computation can be performed. The spikes in the AASHTO curve tend to correspond with

spikes in the other curves, so the influence of the horizontal geometry can certainly be observed in both methods. The AASHTO method can be seen to under-predict sight distance most of the time, but it can also over-predict sight distance, which is a dangerous situation. Judging by these results, it would be wise to use a more robust 3-D method for design problems where sight distance is an important factor. The old 3-D method is not bad; it merely represents a conservative estimate. The newer method allows for the prediction of greater sight distances when the geometry so warrants.

4. Conclusions

This paper demonstrates a new 3-D sight distance estimation method based on a combination of a 3-D spline interpolation borrowing from a physical analogy with the structural mechanics of thin plates, and a truncated search algorithm similar to methods proposed elsewhere in the literature. The methodology incorporates all of the most common design elements from horizontal alignment design, vertical design, and lateral roadway features. The spline computation can be performed by numerical linear algebra, which is relatively simple, but the accuracy of the results improves as the problem is sub-divided. It is advised to build in overlaps between adjoining sections when sub-dividing the problem to assure consistency between the results.

The method compares favorably against existing 3-D methods, and is shown to be less conservative in estimating sight distance in those situations where the combination of vertical and horizontal geometry warrants it. It is considerably more accurate than the simple 2-D methods typically shown in textbooks and the most common design references.

One of the most restrictive elements of sight distance at night is headlight sight distance, which is not considered in this paper. It should be quite possible to build an additional set of criteria into the model that constrain the sight lines to within the visible range of headlights at night, and this would provide a marked practical improvement in the model. Other modifications could include the consideration of design elements such as tunnels, ramps, bridges, and overpasses. It would also be interesting to compare empirical safety measurements at locations known to have actual sight distances significantly higher or lower than what is prescribed, to see what effect these deviations can have in an operational setting.

REFERENCES

1. Hassan, Y., Easa, S. M., and Abd El Halim, A. O. (1995). Sight distance on horizontal alignments with continuous lateral obstructions. Transportation Research Record 1500, pp. 31-42. Transportation Research Board, Washington, DC.
2. American Association of State Highway and Transportation Officials (AASHTO) (2001). *A policy on geometric design of highways and streets*, Washington, DC.
3. Hassan, Y., Easa, S. M., and Abd El Halim, A. O. (1995). Sight distance on horizontal alignments with continuous lateral obstructions. Transportation Research Record 1500, pp. 31-42. Transportation Research Board, Washington, DC.
4. Easa, S.M. (1993). Lateral clearance needs on compound horizontal curves. Journal of Transportation Engineering, 119(1), pp. 111–123.
5. Easa, S.M. (1994). Design considerations for highway reverse curves. Transportation Research Record 1445, pp. 1-11. Transportation Research Board, Washington, DC.
6. Lovell, D.J. (1999). Automated calculation of sight distance from horizontal geometry. Journal of Transportation Engineering 125(4), pp. 297-304.

7. Lovell, D.J., J.C. Jong, and P.C. Chang (2001). Improvements to sight distance algorithm. Journal of Transportation Engineering, 127(4), pp. 283-288.
8. Easa, S.M. (1991a). Sight distance model for unsymmetrical crest curves, Transportation Research Record 1303, pp. 39-50. Transportation Research Board, Washington, DC.
9. Easa, S.M. (1991b). Sight distance model for unsymmetrical sag curves, Transportation Research Record 1303, pp. 51-62. Transportation Research Board, Washington, DC.
10. Hassan, Y., Easa, S. M., and Abd El Halim, A. O. (1996). Analytical model for sight distance analysis on three-dimensional highway alignments. Transportation Research Record 1523, pp. 1-10, Transportation Research Board, Washington, DC.
11. Ismail, K. and Sayed, T. (2007). New algorithm for calculating 3D available sight distance. Journal of Transportation Engineering, 133(10), pp. 572-581.
12. Nehate, G. and Rys, M. (2006). 3D calculation of stopping sight distance from GPS data. Journal of Transportation Engineering, 132(9), pp. 691-698.
13. Duchon, J. (1976). Interpolations des fonctions de deux variables suivant le principe de la flexion des plaques minces. RAIRO Analyse Numérique, 10, pp. 5-12.
14. Bookstein, F.L. (1989). Principal warps: Thin-plate splines and the decomposition of deformations. IEEE Transactions on Pattern Analysis and Machine Intelligence, 11(6), pp. 567-585.